Atmospheric Diabatic Heating in Different Weather States and the General Circulation

WILLIAM B. ROSSOW

CREST Institute at the City College of New York, New York, New York

YUANCHONG ZHANG

Applied Physics and Applied Mathematics, Columbia University, New York, New York

GEORGE TSELIOUDIS

NASA Goddard Institute for Space Studies, New York, New York

(Manuscript received 29 October 2015, in final form 15 December 2015)

ABSTRACT

Analysis of multiple global satellite products identifies distinctive weather states of the atmosphere from the mesoscale pattern of cloud properties and quantifies the associated diabatic heating/cooling by radiative flux divergence, precipitation, and surface sensible heat flux. The results show that the forcing for the atmospheric general circulation is a very dynamic process, varying strongly at weather space–time scales, comprising relatively infrequent, strong heating events by ''stormy'' weather and more nearly continuous, weak cooling by ''fair'' weather. Such behavior undercuts the value of analyses of time-averaged energy exchanges in observations or numerical models. It is proposed that an analysis of the joint time-related variations of the global weather states and the general circulation on weather space–time scales might be used to establish useful ''feedback like'' relationships between cloud processes and the large-scale circulation.

1. Introduction

The latitudinal variation of solar heating of Earth produces a coupled atmosphere–ocean general circulation that transports heat poleward, lowering temperatures at lower latitudes and raising them at higher latitudes. The corresponding changes in the thermal radiative cooling result in radiative exchanges at the top of the atmosphere (TOA) that are locally out of balance: net radiative heating of lower latitudes and net radiative cooling at higher latitudes. The coupling of the atmosphere–ocean circulations is primarily mediated by water processes: evaporative cooling of the surface and precipitation heating of the atmosphere. The latter is produced by the atmospheric motions themselves, which also produce clouds that alter the radiation exchanges. Together, precipitation and the cloud-induced radiation changes feed back on the general circulation. We can only observe the final result of the simultaneous action of all these processes and we cannot observe the circulation without these feedbacks, so we are not able to quantify them directly from observations.

The ''missing link'' in understanding and representing clouds and cloud process feedbacks accurately in numerical general circulation models (weather and climate) has always been how to relate the smaller-scale cloud processes to the small-scale and much larger-scale atmospheric motions that cause them. The time variability of this connection spans the whole range of scales constituting weather events. In other words, cloud variability is essentially fluid dynamical in character (the time derivative is significant), so the process relationships cannot be represented by (separately) space–time-averaged quantities. To unravel this complex set of interactions and their scale-dependent time variations, we might look for some way to reduce the problem to ''simpler'' situations. One way to do this might be to identify distinctive subsets of the observations (states of the atmosphere), where the physical relationships for members in a subset are more similar to each other than they are to the members of a

Corresponding author address: William B. Rossow, CREST Institute at the City College of New York, Steinman Hall (T-107), 140th Street and Convent Avenue, New York, NY 10031.
E-mail: wbrossow@gmail.com

DOI: 10.1175/JCLI-D-15-0760.1

different subset. Then averaging over each subset better represents the relationships within them and between subsets than averaging over all the observations and mixing the different situations together. If these subsets (weather states) can be identified and their typical characteristics quantified, then variations of the processes with variations of the atmospheric circulation might usefully be approximated solely by changes from one state to another, providing a simpler representation of time variations and feedbacks. Such an analysis approach has to be applied to long time records of global observations to ensure a complete sample of situations with robust statistics.

The weather and its changes have been associated with characteristic cloud property distribution patterns, which we call weather states (Jakob and Tselioudis 2003; Rossow et al. 2005; Tselioudis et al. 2013). Previous studies have shown (so far) that these weather states (or cloud regimes) are associated with distinct conditions in the atmosphere (e.g., Jakob et al. 2005; Haynes et al. 2011; Davies et al. 2013), exhibit distinctive composite TOA radiative fluxes (Oreopoulos and Rossow 2011; Tselioudis et al. 2013), and have very different tropical precipitation rates (Jakob and Schumacher 2008; Lee et al. 2013; Rossow et al. 2013). Tselioudis et al. (2013) extended the earlier regional studies to a set of global weather states (GWS) and showed additionally that they exhibit characteristic cloud vertical structures and are associated with characteristic mean atmospheric vertical motions. We propose that these GWS and their composite atmospheric diabatic heating should be used to explore whether they can represent the connection between the time variations of the cloud processes and the atmospheric circulation.

2. Data and methods

The data products used here are as follows. The GWS (Tselioudis et al. 2013) are based on 26.5 years of ISCCP D-version global cloud products that provide 3-hourly (daytime only) joint histograms of cloud-top pressure and optical thickness (Rossow and Schiffer 1999). The radiative flux divergences (FD) are from the ISCCP-FD product that uses the ISCCP cloud products, together with ancillary surface and atmosphere products, to calculate global, 3-hourly radiative flux profiles at five levels (Zhang et al. 2004). The precipitation comes from the 3-hourly TRMM Multisatellite Precipitation Analysis (TMPA or 3B42) product (Huffman et al. 2007), where missing values at latitudes poleward of 50° are filled using the GPCP One-Degree Daily (1DD) product (Huffman et al. 2001) by distributing the daily precipitation equally over 3-hourly intervals within each day. The ocean surface fluxes of sensible heat come from the Air–Sea Turbulent Flux dataset (SeaFlux), version 1.0 (Clayson et al. 2012), and the land surface fluxes can be found online (http://hydrology.princeton.edu/data/landflux/; see Vinukollu et al. 2011). The reviews by L'Ecuyer et al. (2015) and Rodell et al. (2015) of these and other data products quantifying energy and water exchanges, respectively, provide estimates of their uncertainties: for monthly mean fluxes, the rough magnitude of the differences among these products is about 10%–15% of their mean values. Since the agreement for TOA mean radiative fluxes is much better than this (cf. Raschke et al. 2016), the uncertainty in atmospheric diabatic heating is about the same as for surface fluxes.

To provide globally complete results, the GWS dataset needs to have the missing nighttime and winter polar region values filled before matching all the datasets. The GWS are filled for each grid cell over the nighttime interval by replicating the previous and subsequent GWS to the middle of the interval. The unilluminated polar regions have GWS replicated from the nearest available time. This changes the relative frequency of occurrence (RFO) values only slightly from the original results. Table 1 shows the RFO (%) of the 12 GWS (filled) defined by the joint histograms shown in Fig. 1, together with an all-clear situation [see Tselioudis et al. (2013) for a detailed interpretation of the GWS] and the average of matched atmospheric heating/cooling rates ($K\,day^{-1}$; roughly equivalent to a net flux of $100\,W\,m^{-2}$) by precipitation, net atmospheric radiation, and surface sensible heat flux. Note that only four of the GWS (1, 2, 3 and 6) have a positive cloud radiative effect and that the first three GWS also have the largest precipitation rates [cf. more discussion in Oreopoulos and Rossow (2011), who used an earlier set of weather states that are very similar to the GWS as discussed in Tselioudis et al. (2013)]. Also shown is the total heating for each GWS (sum of the three contributions) times its RFO. The time period covered by the matched data is 1998–2007 (10 yr of global, 3-h data).

3. Results

Figure 2 shows the zonal mean RFO (for the 10-yr period) for four groups of GWS that dominate the heating/cooling in the different parts of the mean atmospheric circulation that define the familiar climate regimes: tropics (GWS 1, 3, 6, and 7), subtropics (GWS 8, 10, and 12), midlatitudes (GWS 2, 5, 9, and 11), and polar regions (GWS 4 and 7). Most of the GWS are concentrated in one (or two) of the climate regimes, whereas GWS 7 is nearly ubiquitous except in midlatitudes. We show GWS 7 in only two of the three

TABLE 1. RFO (%) of the 12 GWS and the composite atmospheric heating/cooling (K day^{-1}; roughly equivalent to a net flux of 100 W m^{-2}) by precipitation, net radiative flux divergence, and surface sensible heat flux. The total heating is the sum of the three contributions times the RFO.

GWS	RFO	Precipitation	Net radiative flux divergence	Surface sensible heat flux	Total
1	4.1	+5.64	−0.52	+0.12	+0.213
2	6.5	+1.40	−0.88	+0.20	+0.047
3	8.4	+1.19	−0.82	+0.13	+0.042
4	5.5	+0.43	−1.08	+0.36	−0.016
5	13.0	+0.45	−1.00	+0.25	−0.040
6	7.3	+0.44	−0.78	+0.15	−0.015
7	32.4	+0.26	−1.06	+0.15	−0.211
8	8.8	+0.18	−1.05	+0.22	−0.058
9	3.7	+0.19	−1.14	+0.12	−0.030
10	5.7	+0.18	−1.19	+0.17	−0.049
11	2.5	+0.15	−1.24	+0.21	−0.022
12	2.1	+0.02	−1.10	+0.15	−0.019

groups where it is frequent but include it in all of the budgets. Figure 3 shows the zonal mean total heating/cooling rates of these GWS multiplied by their RFO. Adding the separate contributions of the particular GWS in each group gives the zonal mean total heating for the groups shown in Fig. 4. Defining the tropics as ±15° latitude, the subtropics as ±15°–35°, the midlatitudes as ±35°–65°, and polar as ±65°–90° (based on Figs. 2 and 3), we find that the total net heating of the tropics is +0.169 K day^{-1}, the subtropics

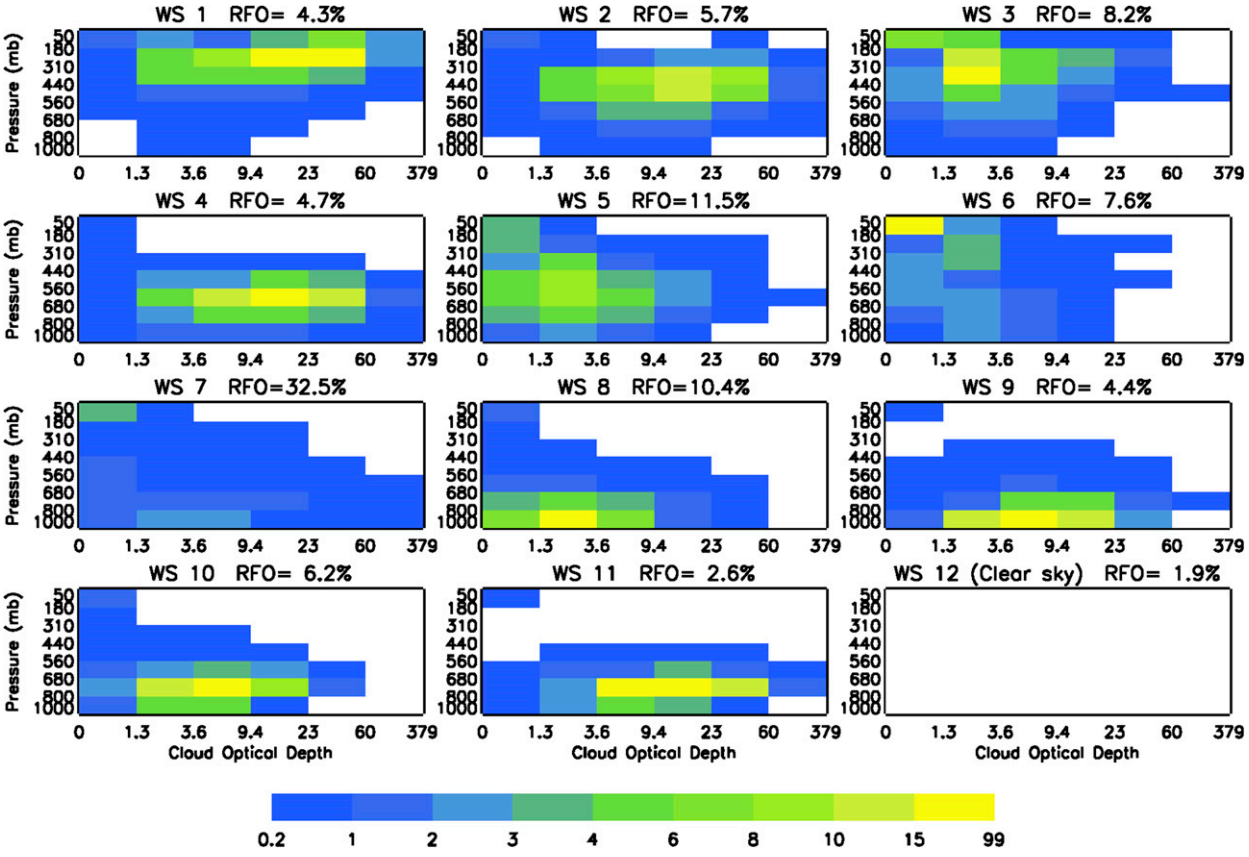

FIG. 1. The joint distributions of cloud-top pressure and optical thickness that define the 11 GWS cloud patterns, plus a 12th state that is totally clear (from Tselioudis et al. 2013). The colors represent the cloud fraction occurring for each combination of cloud properties. Above each histogram are the GWS number and its global (original) RFO.

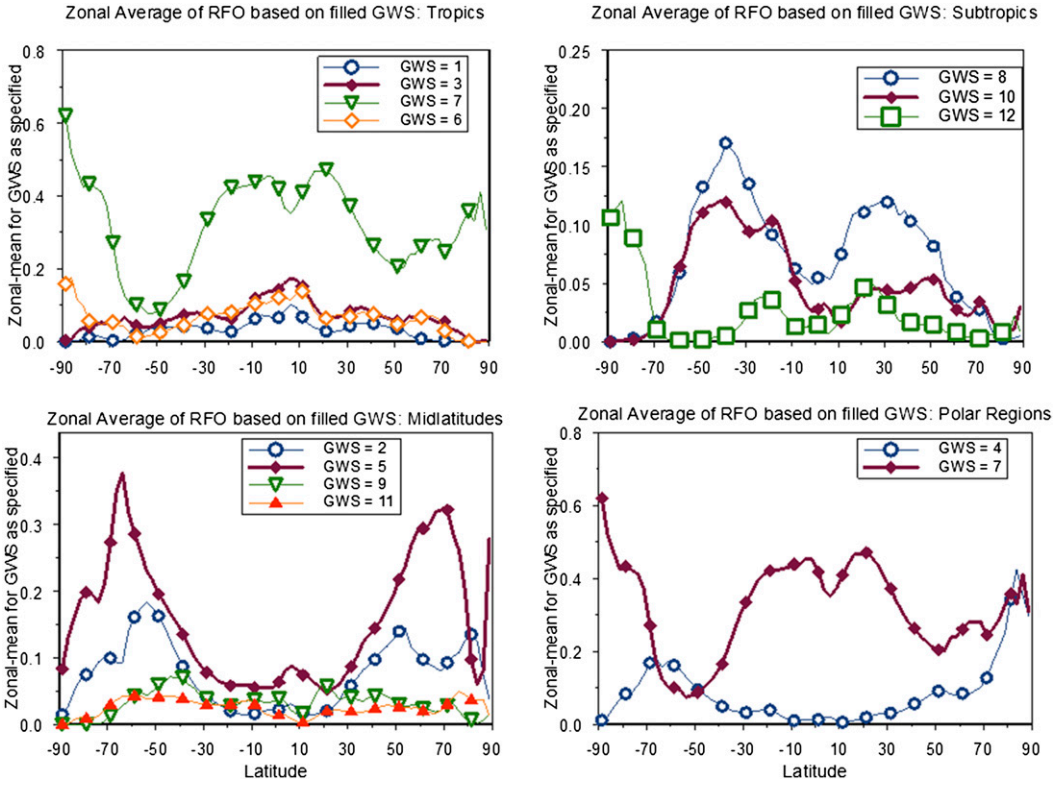

FIG. 2. Time and zonal mean RFO of the GWS divided into four groups associated with four climate regimes: tropics, subtropics, midlatitudes, and polar regions. The RFO values (filled) are shown for all latitudes despite the focus on a particular latitude range in each group; not all GWS are shown in each panel and GWS 7 is shown twice.

is $-0.338\,\mathrm{K\,day^{-1}}$, midlatitudes is $-0.196\,\mathrm{K\,day^{-1}}$, and polar is $-0.375\,\mathrm{K\,day^{-1}}$ (if these values are weighted by relative area, they become +0.169, −0.306, −0.126, and $-0.081\,\mathrm{K\,day^{-1}}$, respectively). The global total RFO-weighted heating for all GWS is $-0.157\,\mathrm{K\,day^{-1}}$. This closure imbalance (roughly $15\,\mathrm{W\,m^{-2}}$) is about the same magnitude, relative to the total heating and cooling rates considered separately, as estimated for the surface energy and water exchange products (L'Ecuyer et al. 2015; Rodell et al. 2015). Note that since GWS 7 is global in extent, its composite heating (area-weighted average) is a mixture of low- and high-latitude conditions, so that it somewhat overestimates the low-latitude cooling [by underestimating solar zenith angle and thus shortwave (SW) absorption and by overestimating temperature and thus longwave (LW) emission] and underestimates high-latitude cooling (overestimates SW absorption and underestimates LW emission). These biases in the composite GWS 7 heating/cooling may explain part of the excess cooling in the global average because the tropical overestimate outweighs the polar underestimate. In the following, we highlight the essential heating/cooling processes summarized in zonal-averaged terms to relate them to the general circulation.

The heating of the tropics is produced by two very low-frequency events (RFO sum about 10%): about 80% of the heating is produced by mesoscale-organized deep convection (GWS 1), with another 20% from more frequent ordinary convection (GWS 3). Two-thirds of the cooling is produced under "persistent" (i.e., RFO about 30%) fair weather conditions (GWS 7) comprising a mixture of boundary layer cumulus and thin cirrus with large amounts of clear sky. (These and subsequent proportions are estimated from the zonal averages of the heating and cooling contributions by the dominant GWS.) The notable points are that the heating and cooling weather states are offset in mean latitude with heating closer to the equator than cooling and that they have very different space–time frequencies (Figs. 2 and 3): very intermittent large heating events are offset approximately by nearly continuous small cooling. As expected, the time-averaged net balance of the whole tropics is positive.

The other part of the Hadley circulation, the subtropics, shows a strong net cooling as expected. Although there is a small amount of heating by precipitation, the surface sensible heat flux is an equally important contribution to heating in these zones. The dominant weather states (other than GWS 7), namely GWS 8, 10, and 12, which comprise

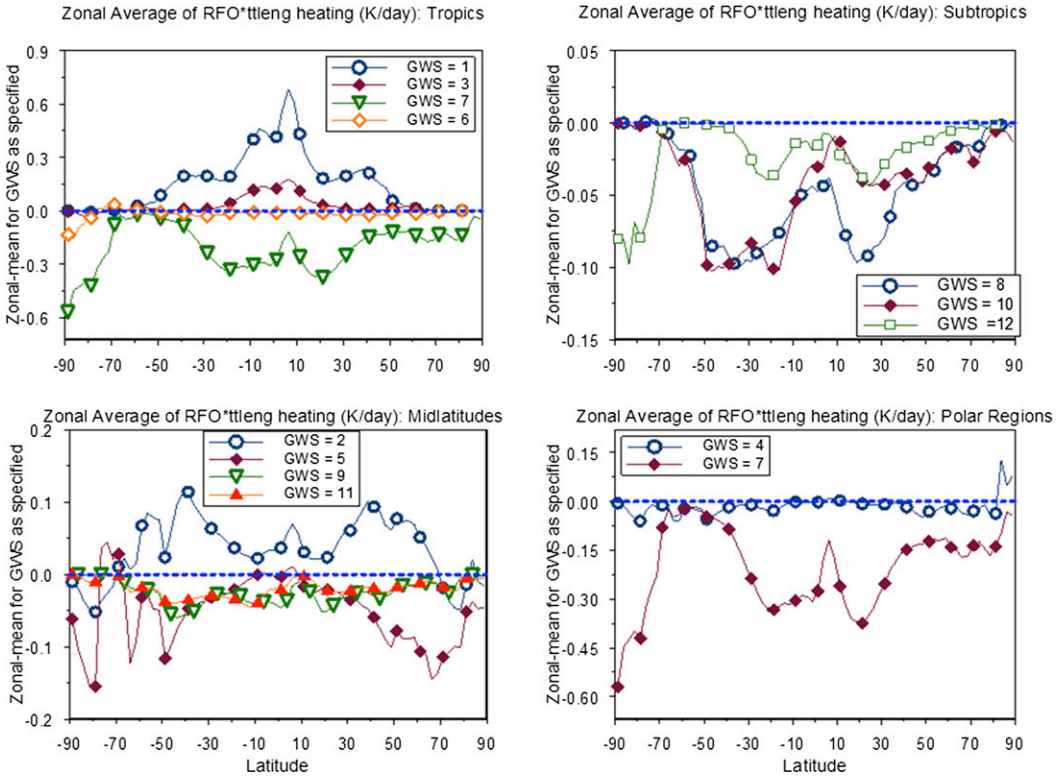

FIG. 3. Time and zonal mean total (RFO weighted) atmospheric diabatic heating/cooling (K day^{-1}) by the particular GWS in the four groups shown in Fig. 2.

broken (cumulus) and extensive (stratocumulus) boundary layer clouds and clear conditions, are dominated by radiative cooling and produce 40% of the total cooling. GWS 7 produces the rest.

The polar regions show the expected strong net cooling produced by the fair weather state (GWS 7), especially over Antarctica where the completely clear state (GWS 12) is also prevalent, and a small contribution from a distinctive high-latitude weather state (GWS 4) that is comprised of low- and midlevel clouds with moderate to large optical thicknesses exhibiting radiative cooling that exceeds its precipitation heating by about a factor of 2. These three weather states together produce a strong net atmospheric cooling. The asymmetry of the situation at the two poles is notable. There is very little totally clear condition (GWS 12) at the North Pole and the RFO of GWS 7 is only about 30% there (GWS 7 contains a large fraction of clear conditions; cf. Tselioudis et al. 2013), whereas at the South Pole the RFO of GWS 12 is nearly 15% and that of GWS 7 is about 50%. Hence the atmospheric cooling at the South Pole is about 3 times stronger than at the North Pole.

In the midlatitudes GWS 2 (deep convection and nimbostratus) produces net heating (precipitation heating $>$ radiative cooling even though the cloud radiative effect is positive) and GWS 5 (optically thinner midlevel clouds) produces net cooling (precipitation heating $<$ radiative cooling), reinforced by the net cooling of two low cloud weather states (GWS 9 and 11) that are generally optically thicker than the subtropical low cloud states. Again the mean latitudinal location of the peak heating is equatorward of the peak cooling (Figs. 2 and 3). Haynes et al. (2011), who used an earlier version of these weather states that is very similar to that used here (see Tselioudis et al. 2013), noted the relative shift of these two weather states for Southern Hemisphere midlatitudes (their states S7 $\approx$ GWS 2 and S5 $\approx$ GWS 5). Using collocated and coincident *CloudSat*/*CALIPSO* profiles confirms that GWS 2 (S7) is a deep extensive cloud (nimbostratus) and that GWS 5 (S5) is a mixture of low- and midlevel clouds. They also find that GWS 2 is associated with predominantly upward and poleward atmospheric motions and positive thermal advection, suggesting a concentration of this GWS in the ''warm sector'' portion of midlatitude cyclones. Likewise, the type of clouds in GWS 5 suggests that it is in the ''cold sector'' portion of midlatitude cyclones (cf. Lau and Crane 1995). Despite significant precipitation heating by GWS 5, this weather state still produces more than half of the total cooling in this regime.

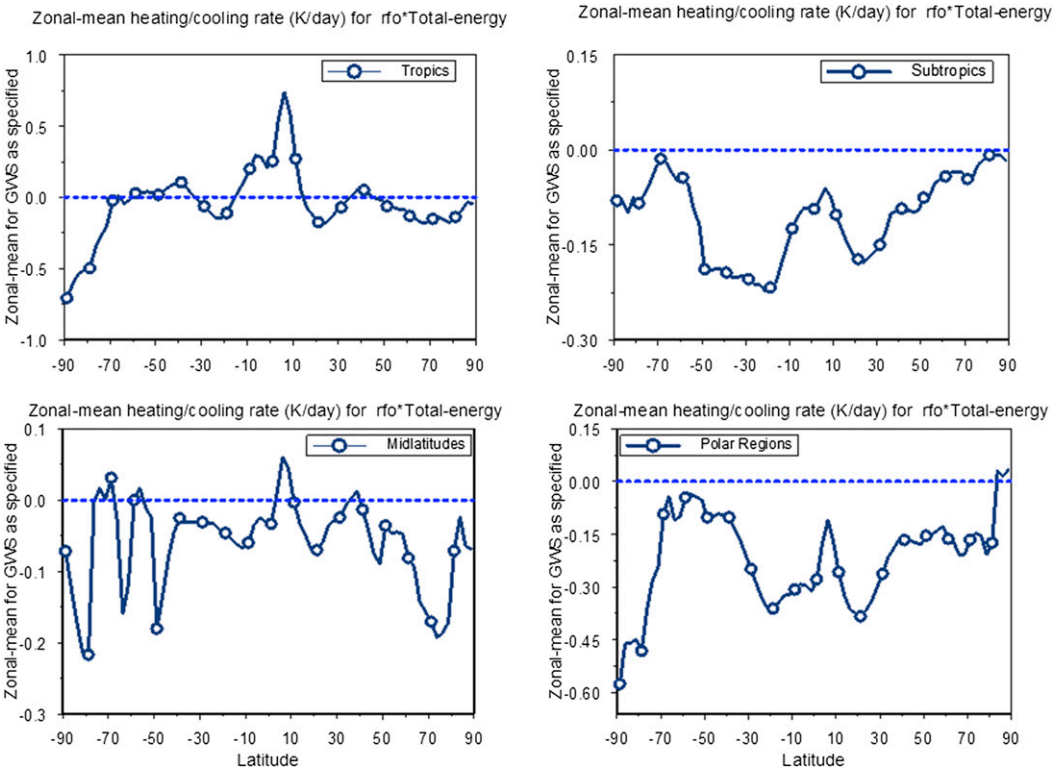

FIG. 4. Time and zonal mean total atmospheric diabatic heating/cooling (K day^{-1}) by the RFO-weighted sum of the contributions of the particular GWS for each group.

4. Discussion

The net atmospheric heating in each of the four climate regimes (Fig. 4) involves only a few of the 12 GWS, corresponding to ''stormy'' heating opposed by ''fair weather'' cooling with the exception of the subtropics, where the most frequent GWS are all fair weather cooling. In each case the stormy weather states are distinctive for that climate regime and occur much less frequently than the fair weather states. Considering the Hadley circulation zone overall, the intermittent net heating near the equator is juxtaposed with persistent net cooling in the tropics and subtropics. In the midlatitudes, the heating GWS again occurs much less frequently than the cooling GWS, but the two dominant weather states (GWS 2 and 5) appear to be associated with different parts of the baroclinic wave systems in midlatitudes, indicating a complex and dynamic relationship of the weather-generated cloud processes with the mean atmospheric circulation. This suggests extending this type of analysis beyond zonal averages to encompass the ''eddy'' aspects of the general circulation. In summary, the atmosphere's energy state is not a static imbalance—the time derivative on weather time scales can be significant, so the analysis of interaction of cloud processes and the atmospheric circulation has to resolve the time variations.

When looked at on weather scales (here 300 km, 3 h), there are very specific cloud property patterns that are produced by the different weather conditions in each major regime of the large-scale general circulation. These patterns are, in turn, related to specific types of diabatic heating (''stormy'') and cooling (''fair weather'') events that are different for each zone and occur with very different space–time frequencies of occurrence. Characterizing the GCM representation of these events and their diabatic heating/cooling in this same way should help better understand how to improve the models. Important topics for further study are GWS vertical structures, different time scales of GWS variation and time-resolved energy (and water budgets). The preliminary results suggest that combining this 10-yr record of GWS and their composite diabatic heating (representing the cloud processes) with a reanalysis of the atmospheric circulation at subdaily time scales can be used to investigate joint time-related variations to establish ''feedback like'' relationships.

Acknowledgments. WBR is supported by grants from the NSF (AGS-1240643) and NASA (NNX13AO39G),

and Y-CZ is supported by the NASA grant. GT is supported by the NASA Modeling, Analysis and Prediction (MAP) program. We thank Christian Jakob for many good discussions of these ideas.

REFERENCES

Clayson, C. A., J. B. Roberts, and A. S. Bogdanoff, 2012: The SeaFlux Turbulent Flux Dataset version 1.0 documentation. SeaFlux Project, 5 pp. [Available online at http://seaflux.org/seaflux_data/DOCUMENTATION/SeaFluxV1.0Documentation.pdf.]

Davies, L., C. Jakob, P. May, V. V. Kumar, and S. Xie, 2013: Relationships between the large-scale atmosphere and the small-scale state for Darwin, Australia. *J. Geophys. Res. Atmos.*, **118**, 11 534–11 545, doi:10.1002/jgrd.50645.

Haynes, J. M., C. Jakob, W. B. Rossow, G. Tselioudis, and J. Brown, 2011: Major characteristics of Southern Ocean cloud regimes and their effects on the energy budget. *J. Climate*, **24**, 5061–5080, doi:10.1175/2011JCLI4052.1.

Huffman, G. J., R. F. Adler, M. Morrissey, D. T. Bolvin, S. Curtis, R. Joyce, B. McGavock, and J. Susskind, 2001: Global precipitation at one-degree daily resolution from multisatellite observations. *J. Hydrometeor.*, **2**, 36–50, doi:10.1175/1525-7541(2001)002<0036:GPAODD>2.0.CO;2.

——, and Coauthors, 2007: The TRMM Multisatellite Precipitation Analysis (TMPA): Quasi-global, multi-year, combined-sensor precipitation estimates at fine scales. *J. Hydrometeor.*, **8**, 38–55, doi:10.1175/JHM560.1.

Jakob, C., and G. Tselioudis, 2003: Objective identification of cloud regimes in the tropical western Pacific. *Geophys. Res. Lett.*, **30**, 2082, doi:10.1029/2003GL018367.

——, and C. Schumacher, 2008: Precipitation and latent heating characteristics of the major tropical western Pacific cloud regimes. *J. Climate*, **21**, 4348–4364, doi:10.1175/2008JCLI2122.1.

——, G. Tselioudis, and T. Hume, 2005: The radiative, cloud and thermodynamic properties of the major tropical western Pacific cloud regimes. *J. Climate*, **18**, 1203–1215, doi:10.1175/JCLI3326.1.

Lau, N.-C., and M. W. Crane, 1995: A satellite view of the synoptic-scale organization of cloud properties in midlatitude and tropical circulation systems. *Mon. Wea. Rev.*, **123**, 1984–2006, doi:10.1175/1520-0493(1995)123<1984:ASVOTS>2.0.CO;2.

L'Ecuyer, T. S., and Coauthors, 2015: The observed state of the energy budget in the early twenty-first century. *J. Climate*, **28**, 8319–8346, doi:10.1175/JCLI-D-14-00556.1.

Lee, D., L. Oreopoulos, G. J. Huffman, W. B. Rossow, and I.-S. Kang, 2013: The precipitation characteristics of ISCCP tropical weather states. *J. Climate*, **26**, 772–788, doi:10.1175/JCLI-D-11-00718.1.

Oreopoulos, L., and W. B. Rossow, 2011: The cloud radiative effect of ISCCP weather states. *J. Geophys. Res.*, **116**, D12202, doi:10.1029/2010JD015472.

Raschke, E., S. Kinne, W. B. Rossow, P. W. Stackhouse, and M. Wild, 2016: Comparison of radiative energy flows in observational datasets and climate modeling. *J. Appl. Meteor. Climatol.*, **55**, 93–117, doi:10.1175/JAMC-D-14-0281.1.

Rodell, M., and Coauthors, 2015: The observed state of the water cycle in the early twenty-first century. *J. Climate*, **28**, 8289–8318, doi:10.1175/JCLI-D-14-00555.1.

Rossow, W. B., and R. A. Schiffer, 1999: Advances in understanding clouds from ISCCP. *Bull. Amer. Meteor. Soc.*, **80**, 2261–2287, doi:10.1175/1520-0477(1999)080<2261:AIUCFI>2.0.CO;2.

——, G. Tselioudis, A. Polak, and C. Jakob, 2005: Tropical climate described as a distribution of weather states indicated by distinct mesoscale cloud property mixtures. *Geophys. Res. Lett.*, **32**, L21812, doi:10.1029/2005GL024584.

——, A. Mekonnen, C. Pearl, and W. Goncalves, 2013: Tropical precipitation extremes. *J. Climate*, **26**, 1457–1466, doi:10.1175/JCLI-D-11-00725.1.

Tselioudis, G., W. B. Rossow, Y.-C. Zhang, and D. Konsta, 2013: Global weather states and their properties from passive and active satellite cloud retrievals. *J. Climate*, **26**, 7734–7746, doi:10.1175/JCLI-D-13-00024.1.

Vinukollu, R. K., E. F. Wood, C. R. Ferguson, and J. B. Fisher, 2011: Global estimates of evapotranspiration for climate studies using multi-sensor remote sensing data: Evaluation of three process-based approaches. *Remote Sens. Environ.*, **115**, 801–823, doi:10.1016/j.rse.2010.11.006.

Zhang, Y.-C., W. B. Rossow, A. A. Lacis, M. I. Mishchenko, and V. Oinas, 2004: Calculation of radiative fluxes from the surface to top-of-atmosphere based on ISCCP and other global datasets: Refinements of the radiative transfer model and the input data. *J. Geophys. Res.*, **109**, D19105, doi:10.1029/2003JD004457.